Expanded View Figures

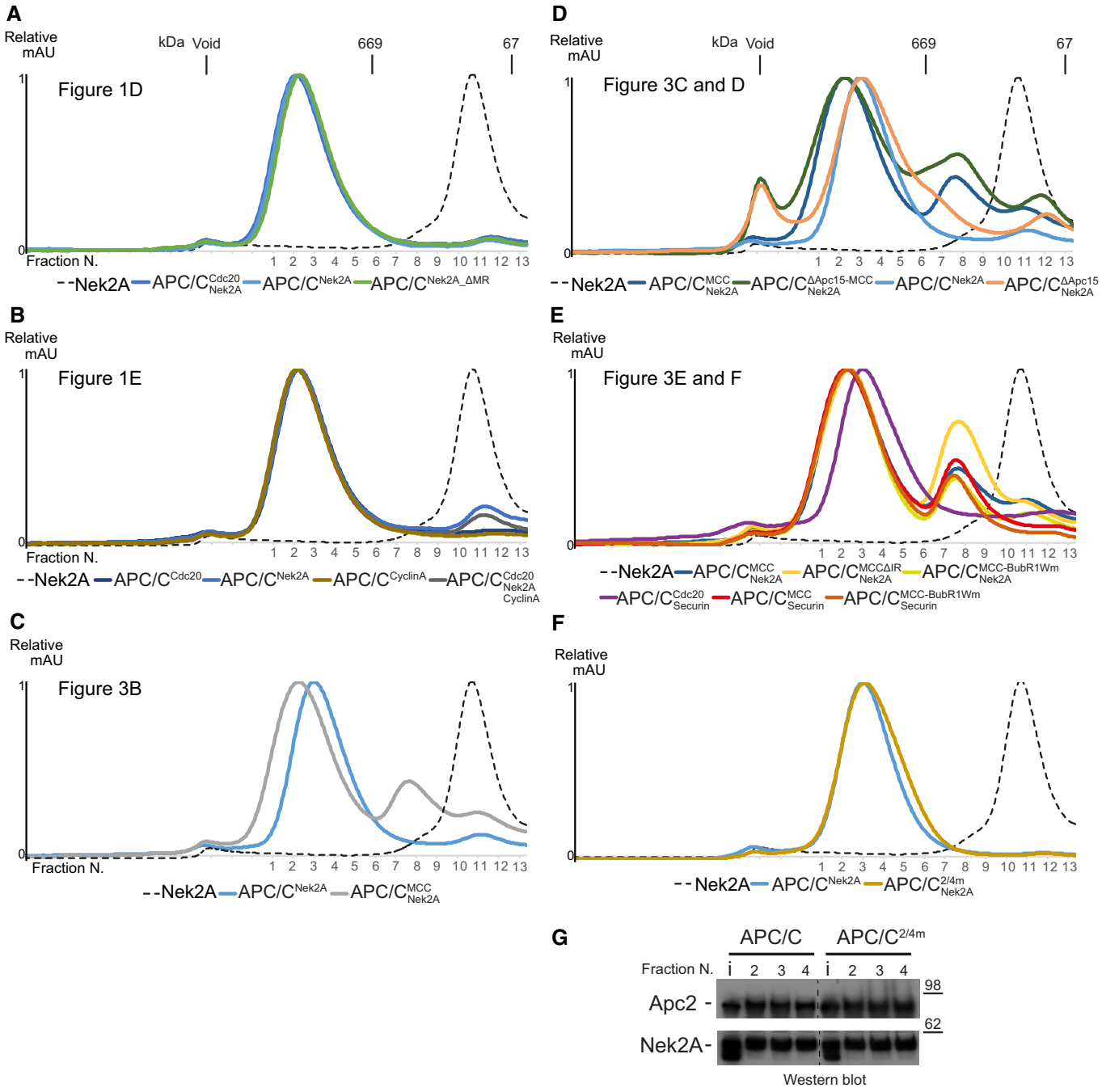

Figure EV1. Binding studies defining the binding mode of Nek2A to the APC/C and APC/C^{MCC} complexes.

A–E Size-exclusion chromatograms of APC/C complexes in this study. The corresponding peak fractions SDS–PAGE gels are shown in the main figures.
F, G Size-exclusion chromatography chromatograms (F) and SDS–PAGE gels (G) of either APC/C wild-type or 2/4 m complexes with Nek2A.

Source data are available online for this figure.

Figure EV2. APC/C–Nek2A complex sample preparation and cryo-EM analysis.

A SDS–PAGE gels (stained with Coomassie blue) of the gel filtration peak fraction from the APC/C–Nek2A complex preparation used in this study. Western blot against Nek2A confirms the presence of the Nek2A 301–406 construct.

B A typical cryo-EM micrograph of APC/C–Nek2A representative of 6,448 micrographs. Scale bar: 500 Å.

C Gallery of two-dimensional class averages of APC/C^{Nek2A} showing different views representative of 50 two-dimensional classes. Scale bar: 150 Å.

D Fourier shell correlation (FSC) curves are shown for all the cryo-EM reconstructions of APC/C^{Nek2A} determined in this study.

E Fourier shell correlation (FSC) curves are shown for all the cryo-EM reconstructions of APC/C^{MCC} determined in this study using cryo-EM data as published [14].

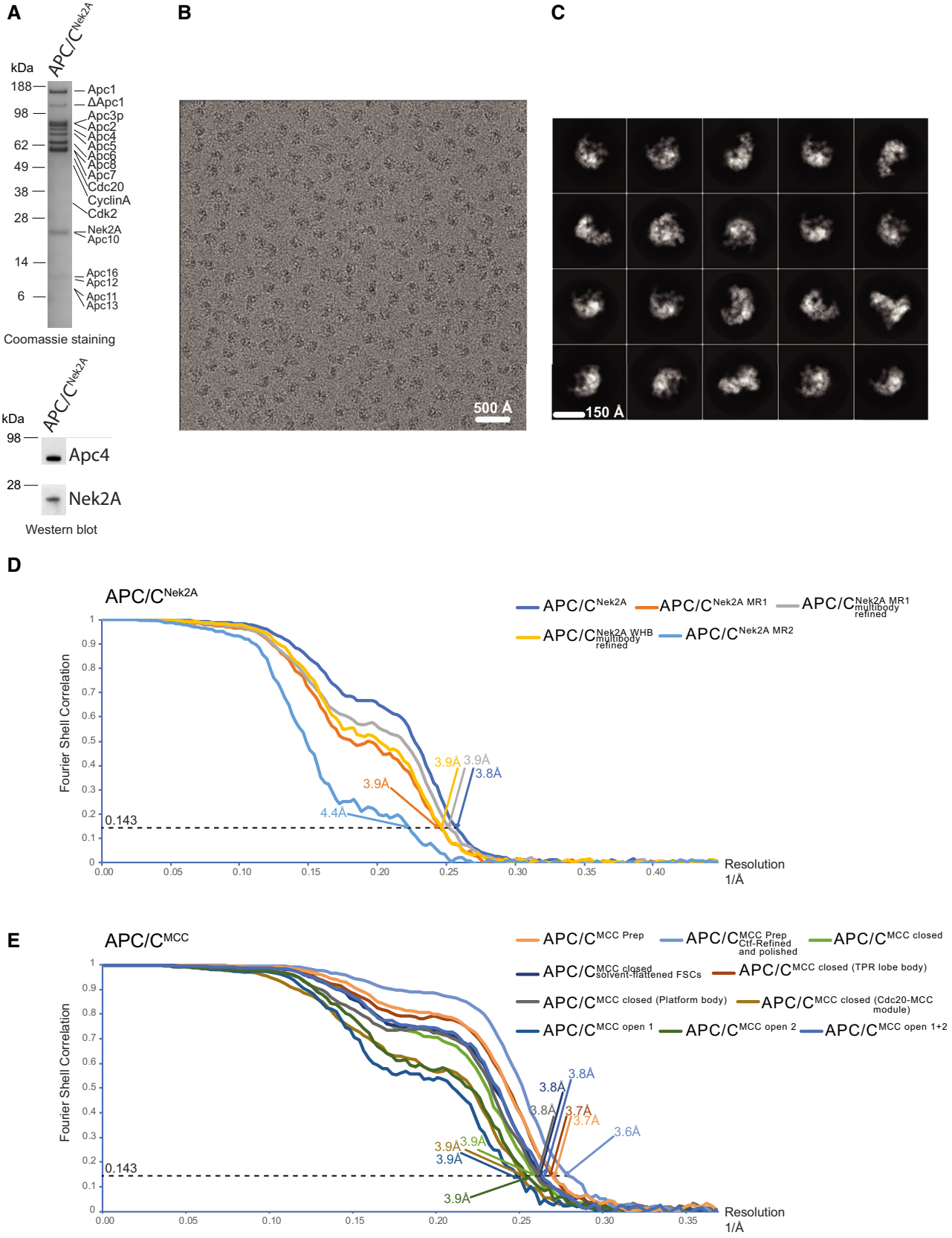
A
APC/C^Nek2A
kDa
188
98
62
49
38
28
14
6
Apc1
ΔApc1
Apc3p
Apc2
Apc4
Apc5
Apc6
Apc8
Apc7
Cdc20
CyclinA
Cdk2
Nek2A
Apc10
Apc16
Apc12
Apc11
Apc13
Coomassie staining
APC/C^Nek2A
kDa
98
28
Apc4
Nek2A
Western blot
B
500 Å
C
150 Å
D
APC/C^Nek2A
APC/C^Nek2A
APC/C^Nek2A MR1
APC/C^Nek2A MR1 multibody refined
APC/C^Nek2A WHB multibody refined
APC/C^Nek2A MR2
Fourier Shell Correlation
0.143
3.9Å
3.9Å
3.8Å
3.9Å
4.4Å
Resolution
1/Å
E
APC/C^MCC
APC/C^MCC Prep
APC/C^MCC Prep Ctf-Refined and polished
APC/C^MCC closed
APC/C^MCC closed solvent-flattened FSCs
APC/C^MCC closed (TPR lobe body)
APC/C^MCC closed (Platform body)
APC/C^MCC closed (Cdc20-MCC module)
APC/C^MCC open 1
APC/C^MCC open 2
APC/C^MCC open 1+2
Fourier Shell Correlation
0.143
3.8Å
3.8Å
3.8Å
3.7Å
3.7Å
3.6Å
3.9Å
3.9Å
3.9Å
3.9Å
Resolution
1/Å

Figure EV2.

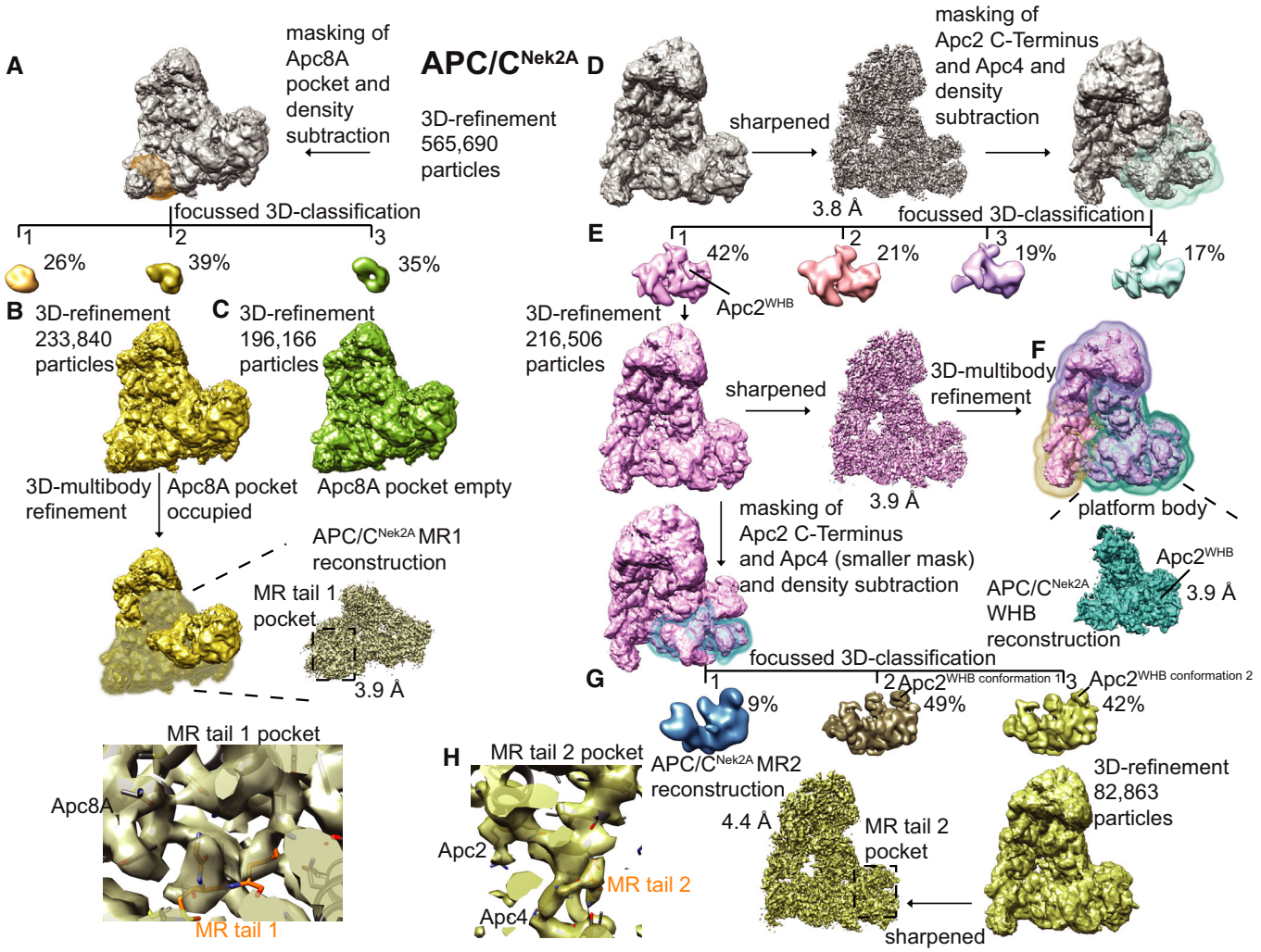

Figure EV3. 3D reconstruction of APC/C–Nek2A complexes.

A–C Workflow for focussed 3D classification and multi-body refinement for 3D reconstruction and refinement of the cryo-EM density for the MR tail 1 binding site on Apc8A.

D–H Workflow for focussed 3D classification and multi-body refinement for 3D reconstruction and refinement of the cryo-EM density for the repositioned APC2^{WHB} domain and for the MR tail 2 binding site on Apc2-Apc4. Classes 2 and 3 shown in (G) differed in the orientation of the APC2^{WHB} domain, and the occupancy of the MR tail 2 was highest in class 3.

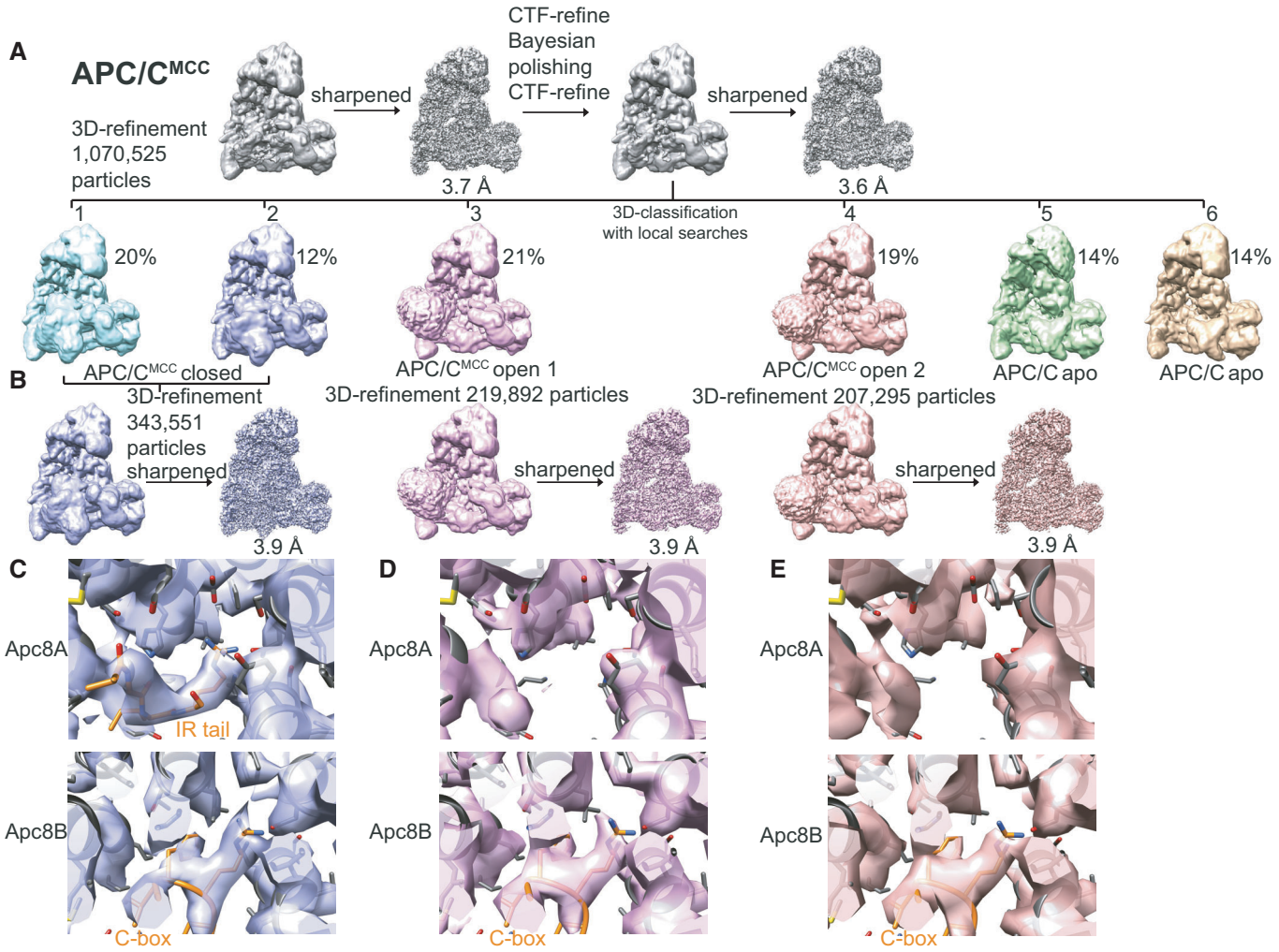

Figure EV4. 3D reconstruction of the APC/C–MCC complex.

A 3D class averages obtained by classification using local searches (see Materials and Methods) are shown for obtaining the APC/C^{MCC} reconstructions.

B Particles from classes 1 and 2 were refined together to obtain the APC/C^{MCC} closed reconstruction. Particles from classes 3 and 4 were separately refined to obtain the APC/C^{MCC} open 1 and 2 reconstructions, respectively. These latter classes were slightly different in the orientation of the Cdc20-MCC module.

C Details of the IR tail and C-box binding site of the APC/C$^{MCC\text{-}closed}$ reconstruction.

D, E (D). Details of the IR tail and C-box binding site of the APC/C$^{MCC\text{-}open-1}$ reconstruction and (E) of the APC/C$^{MCC\text{-}open-2}$ reconstruction. Neither of the two APC/C$^{MCC\text{-}open}$ reconstructions shows clear density for the Cdc20^{MCC} IR tail.

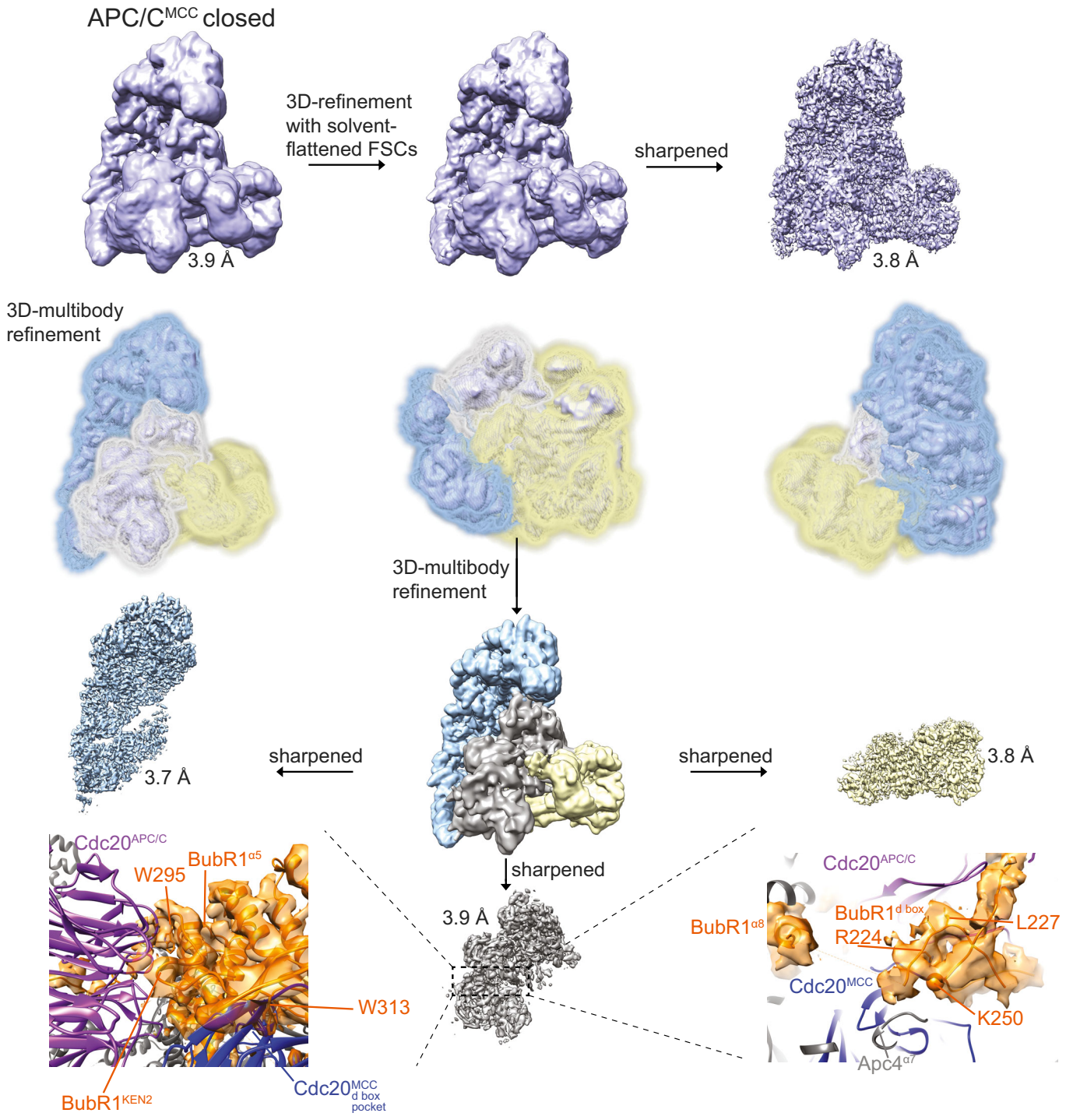

Figure EV5. 3D Multi-body refinement of the APC/C–MCC complex.

3D multi-body refinement strategy for the APC/C$^{MCC\text{-}closed}$ reconstruction (see Materials and Methods). Masks defined for the three APC/C^{MCC} bodies are shown. Details of new BubR1 regions built guided by the improved APC/C^{MCC} cryo-EM map are shown at the bottom. This assignment is consistent with [47–49].